Ultralinear Glucose Sensing Device with Membrane Supported Complementary Split-ring Resonator on SIW

Louis Wai Yip Liu[a]
[a] **Faculty of Engineering, Vietnamese German University, Vietnam**

Abstract

The linearity of a glucose sensor is one of the most important indicators for ensuring measurement accuracy, system stability and post-measurement data processing efficiency. As yet, this issue has not been seriously investigated in the field of glucose sensing. In this work, the use of a substrate-integrated-waveguide (SIW) together with a specially tailored membrane-supported resonator (CSRR) is proposed for realizing an ultra-linear glucose sensor. **Method:** An SIW waveguide with two coplanar ports were realized on an FR4 substrate. On one side of the SIW waveguide, a CSRR was fabricated at the central region, which also served as the sensing region. On the other side of the SIW waveguide, the substrate at the central sensing region was thinned down to a negligible thickness using a nail grinder, thereby forming a circular recess with a membrane-thick bottom for holding a glucose-loaded test solution. The glucose concentration was determined by obtaining the resonant frequency shift in the reflection coefficient (i.e. S11). **Results:** The proposed glucose sensor has exhibited a highly linear correlation between the glucose concentration and the resonant frequency, with a Pearson correlation coefficient (r) reaching 0.99, even though the magnitudes of S11 minima were subjected to ambient electromagnetic interference. The sensitivity was found to be 1.6 MHz/(mg/dL). The resonant frequency was very weakly dependent on the volume of the test solution. **Conclusion:** Overall, the proposed glucose sensor has exhibited not only a high sensitivity but also a highly linear characteristics even in the presence of external electromagnetic interference.

Keywords: membrane, glucose-sensing, metamaterial, SIW, spoof surface plasmon polariton

Introduction

Glucose sensing is currently one of the most popular topics of research. The public perception towards COVID has not only generated renewed research interests in the field of glucose sensing, but also a lot of demands in terms of the quality of a glucose sensing device. In the old days, the research community around the globe focused mainly on the accuracy of a glucose sensor, and any sensing device that satisfies the Clarke Error Grid criteria was usually considered acceptable. Nowadays, due to the practical requirements from the public, and in the wake of the global coronavirus outbreak in 2019, the quality requirements of a glucose sensor are much broader and stricter. Unlike before, not only should we pay attention to the in-

vivo blood glucose measurement, but we should be mindful of the sugar concentration in the food or drink.

Of all the quality requirements under consideration by the research community, the most researched one is perhaps the sensitivity. In recent years, almost all the studies on experimental glucose sensing devices have devoted almost exclusively to sensitivity. What is relatively under-explored is the linearity of a glucose sensor. The linearity of a sensor is one of the important indicators for ensuring measurement accuracy, system stability, and data processing efficiency. Poor linearity in a sensor is an indication that more work will be required to get X if we know Y. With a highly linear glucose sensor, we can (with in reasonable limits) determine the glucose concentration from the measured samples by simple interpolation. If a glucose sensor has a poor linearity, on the other hand, we have to go to greater lengths to determine the glucose concentration when you know just the measured parameters. In general, the more linear the glucose sensor's output, the easier it is to calibrate and to minimize uncertainty in its output scaling.

Lack of linearity frequently occurs in measurement processes. A poorly linear glucose sensor may simply have non-linear elements inside the sensor but this problem is difficult to correct. On the other hand, another more likely cause of non-linearity in a sensor is existence of measurement errors. In a contact-based glucose sensing process, one of the most common causes of errors that leads to non-linearity is volume discrepancy. Most of the experimental contact based glucose sensing device is usually designed to conduct measurements of glucose concentrations for samples of equal volume. When the volume of a sample is slightly different, the measured glucose concentration can be very different from the expected value.

Glucose sensing is undoubtedly a highly important field of science. Although this field has been established for more than a decade, there has not been any serious attempt to resolve the issues of volume discrepancies among different sample. Motivated by this concern, this study attempted to resolve the volume discrepancies among different sample solutions using the concept of spoof surface plasmon polaritons.

Reference	Sensitivity (MHz/(mg/dL))	Lowest Detection Quantity	Methodology	Freq (GHz)	Linearity
[1]	1.218	0.774 mg/dL	SIW	4.65	Not known
[9]	0.42%	100 mg/dL	SIW	3.43	Not known
[10]	0.310	20 mg/dL	SIW	1.7	Not known
[11]	~2 at lowest concentration ~0.4 for concentration	0 mg/dL	CSIW	4.4	Not linear

	range (50 mg/dL - 100 mg/dL)				
[12]	0.25 for concentration range (106 mg/dL - 162 mg/dL) 0.235 for concentration range (162 mg/dL - 196 mg/dL) 0.257 for concentration range (196 mg/dL - 231 mg/dL)	106 mg/dL	SIW	5.36	Not linear
This work	1.6 for all glucose concentrations	0	SIW with membrane-supported CSRR	15.4	Highly linear

Methodology

This section discusses the methodology of this work. To start with, the basic construction of the proposed sensor is first explained. An analysis that justifies the proposed design will be given. Finally, the measurement process focusing on the sensitivity and the linearity will be described in details.

A) Basic Construction of the Proposed Glucose Sensor

The dimensions of the proposed glucose sensor is 26 mm x 8 mm x 1mm. Figs. 1a and 1b show the bottom side of the proposed glucose sensor facing upward. The proposed glucose sensor has been realized in FR4. The bottom of the sensing region was a complementary split ring resonator (CSRR) at the centre of a full-wave resonator realized in substrate-integrated waveguide (SIW). The CSRR was sitting on an ultra-thin FR4 membrane, of which the thickness was no more than 10 microns. The SIW full-wave resonator has a length of exactly 1 guided wavelength of 15.2 GHz. Connected to the input/output ports of the SIW full-wave resonator was coplanar waveguide ports. When used, port 1 is used as a sensing port to be connected to a vector network analyzer (VNA), whilst port 2 is to be terminated with a 50 ohm shunt resistor.

Figs 1c and 1d show the top side of the proposed glucose sensor. The top of the sensing region was a circular recess designed as a container to hold the test solution. In Fig. 1d, the FR4 substrate is made transparent so that the vias are highly visible. During the fabrication process, the circular recess was ground using a finger nail grinder until the bottom of the sensing area was partially transparent (see Fig. 1e for illustration). Under this condition, the depth of the circular recess was slightly less than the thickness of the FR4 substrate, and the bottom of the sensing area was literally an ultra-thin water-proof membrane which not only prevented water leakage but also protected

the CSRR from any form of chemical attacks. According to our measurement, the thickness of this membrane was slightly less than 100 microns.

During the process of a measurement, the circular recess was filled with a glucose-water solution using a mini-pipette until it was fully filled. Port 2 will be terminated with a 50 ohm shunt resistor, whilst the reflection coefficient will be measured at port 1 using a VNA.

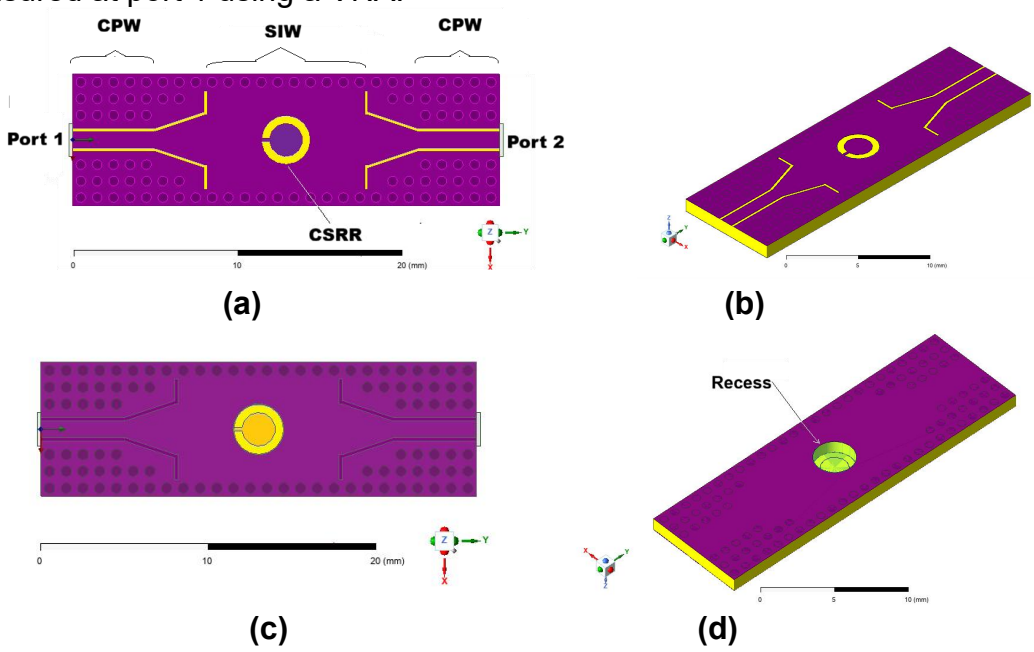

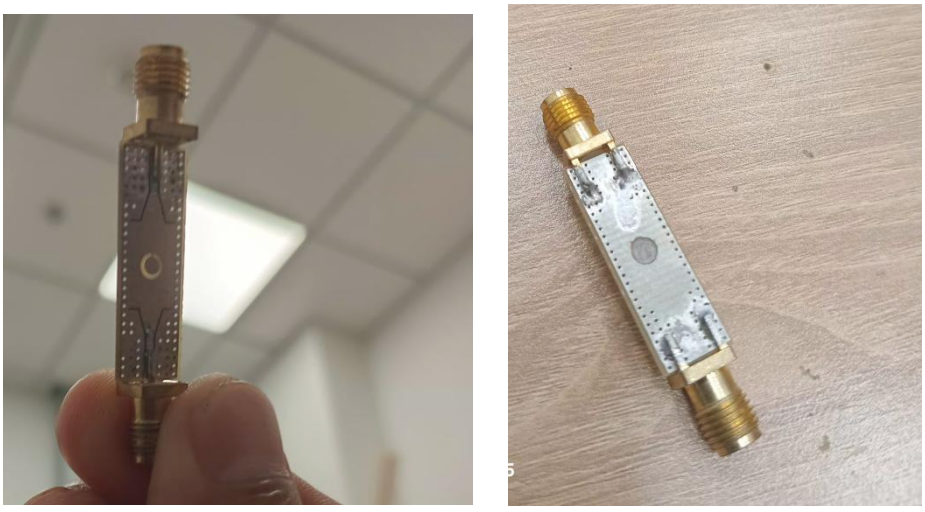
(e) (f)

Figure 1. Construction of the proposed glucose sensor. (a) the bottom view of the glucose sensor; (b) the isometric view of the glucose sensor with the bottom metal facing upward; (c) the top view of the glucose sensor; (d) the isometric view of the glucose sensor with the top metal plate facing upward; (e) the photo showing the top metal plate of the glucose sensor; (f) the photo showing the bottom view of the glucose sensor.

B) Formation of Surface Waves along the FR4/CSRR Interface

At the interface, where $z=0$, the electric fields are continuous, i.e. $E_{dz}(z=0)=E_{mz}(z=0)$ and $E_{dy}(z=0)=E_{my}(z=0)$. Using these boundary conditions, the following well known existence condition of spoof surface polaritons can be obtained:

$$\frac{k_d}{k_m}=-\frac{\varepsilon_d}{\varepsilon_m} \tag{2.1}$$

Substituting $k_d^2=k_y^2-k_o^2\varepsilon_d$ and $k_m^2=k_y^2-k_o^2\varepsilon_m$ into (2.1), we obtain the following dispersion relationship:

$$\frac{k_y}{k_o}=\sqrt{\frac{\varepsilon_m\varepsilon_d}{\varepsilon_m+\varepsilon_d}} \tag{2.2}$$

Equation (2.2) dictates that either ε_m or ε_d should be negative in order to make k_y real and positive. ε_d is positive and cannot be changed because it is the permittivity of the FR4 membrane suspending the CSRR. The only permittivity that is possibly negative is ε_m, which is the permittivity of the CSRR. Metal is considered as a plasma with a permittivity given by:

$$\varepsilon_m = 1 - \frac{\omega_p^2}{\omega^2} \tag{2.3}$$

where $\omega_p$is the plasma frequency of the metal. On the other hand, the CSRR is essentially a diluted plasma, of which the formula for the CSRR's permittivity is of the same form but the plasma frequency $\omega_p$is reduced and obtained as a dual for the split-ring resonator (SRR). By substituting equation (2.3) into (2.2), we obtain:

$$\frac{k_y}{k_o}=\sqrt{\frac{(\omega^2-\omega_p^2)\varepsilon_d}{(\omega^2-\omega_p^2)+\omega^2\varepsilon_d}} \tag{2.4}$$

For the purpose of glucose sensing, the magnitude of the transverse electric field is preferred to be maximized. The transverse electric field is given by:

$$E_z = \pm E_0 \frac{k_y}{k_z} exp\left(j(k_y y + k_z|z|) - \omega t\right) \tag{2.5}$$

In other words, k_y is preferably maximum, whilst k_z is preferably minimum. By setting $k_x\to\infty$ in equation (2.1.16b), which means that $(\omega^2-\omega_p^2)+\omega^2\varepsilon_d$ should be set to zero, we have:

$$\omega=\frac{\omega_p}{\sqrt{1+\varepsilon_d}} \tag{2.6}$$

In equation (2.6), ω is the frequency limit where the velocity of the spoof surface plasmon polariton becomes minimum in the direction of propagation. This frequency limit is commonly known as surface plasma frequency. ω is also the resonant frequency where the combined permittivity along the interface between the CSRR and the FR4 membrane, $\sqrt{(\varepsilon_d\varepsilon_m)/(\varepsilon_d+\varepsilon_m)}$, changes from very positive to very negative. The condition where $\sqrt{(\varepsilon_d\varepsilon_m)/(\varepsilon_d+\varepsilon_m)}$ undergoes such a positive-to-negative transition is commonly known as anomalous dispersion.

It is difficult to use equation (2.6) to obtain the surface plasma frequency without any knowledge of the CSRR's plasma frequency. However, we can still obtain

the resonant frequency of the CSRR using an analytical formula for the conventional split-ring resonator (SRR). According to Babinet's principle of duality [3], the resonance frequencies of a split-ring resonator (SRR) and its complementary counterpart are identical if their corresponding geometries are the same. The major difference between SRR and its counterpart (i.e. CSRR) lies in the fact that SRR gives rise to a bandpass characteristic whilst CSRR gives rise to a bandstop characteristic [4].

Let's apply the modified formula given in [6,7] to Fig. 2a, in which the basic geometry of a dummy SRR is shown. The complementary counterpart of the SRR in Fig. 2a is shown in Fig. 2b. In Fig. 2a, r, w and g respectively stand for the inner-most radius of the circular metal track, the width of the metal track and the gap width. Another parameter that is not shown in Figs 2a and 2b is the metal thickness, h.

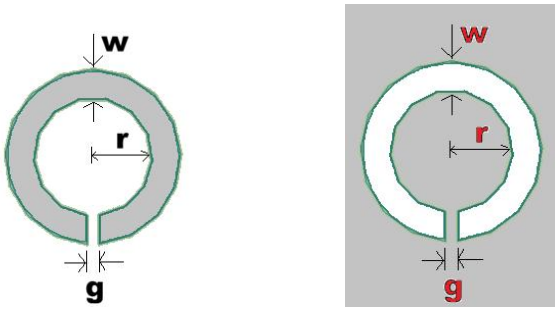

(a) (b)

Fig. 3. Resonators: (a) split-ring resonator; (b) complementary resonator of the same geometry.

The resonant frequency is given by:

$$f_o = \frac{1}{2\pi\sqrt{L_t(C_g+C_{sur})}} \tag{2.7}$$

where L_t is the total inductance of the metallic part given by:

$$L_t = \mu_0(r + 0.5w)\left(ln\left(\frac{r+0.5w}{h+w}\right) - 0.5\right) \tag{2.8}$$

C_g is the capacitance due to the fringing electric in the gap, *g*, given as:

$$C_g = \varepsilon_0\left(\frac{wh}{g} + (h + w + g)\right) \tag{2.9}$$

C_{sur} is the capacitance due to the surface, which is given as:

$$C_{sur} = \frac{2\varepsilon_0 h}{\pi} ln\left(\frac{4r}{g}\right) \tag{3.0}$$

In this study, r, g and w were respectively 1mm, 0.2mm and 0.5mm. The metal thickness, *h*, is approximately 34 microns. With these data substituted to the formula in equation (2.7), By substituting the these data into equation (2,7), we obtain the resonant frequency to be 70.72 GHz. But this frequency ignores the dielectric substance attached to the CSRR, which is the FR4 membrane separating the CSRR and the water column.

The relative permittivity of water at around 15GHz is approximately 38. The thickness of the FR4 membrane (denoted as d_f) was 0.1 mm. The thickness of

the water column (dentoted as d_w) was 1mm. Using Maxwell-Garnett approximation, the aggregate permittivity due to the combination of glucose and the FR4 membrane becomes:

$$\varepsilon_d = (d_d + d_w)\left(\frac{d_f}{\varepsilon_f} + \frac{d_w}{\varepsilon_w}\right)^{-1} \approx 20.9 \quad (3.1)$$

By applying substituting ε_d into equation (2.6), the resonant frequency (or surface plasma frequency) becomes exactly 15.1 GHz. According to the Babinet's principle of duality, this calculated resonant frequency is applicable to not only the SRR in Fig. 3a but also to the CSRR in Fig. 3b

The calculated resonant frequency has been further verified by simulating the structure as shown in Fig. 4a, where two CSRR's are connected back to back on a microstrip line. The simulated performance is shown in Fig. 4b, which has clearly shown that the simulated resonant frequency was 15.9 GHz, as opposed to the calculated value of 15.1 GHz.

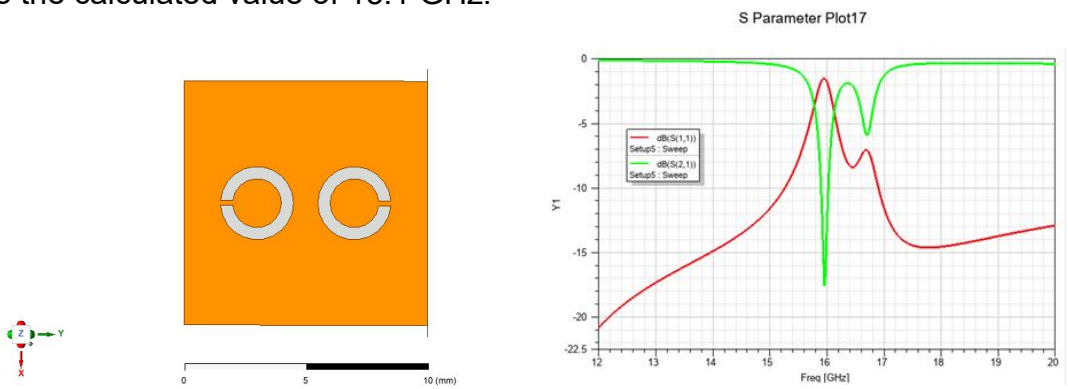

(a) (b)

Fig. 4. Simulation: (a) simulated circuit containing two CSRR's connected back to back on a microstrip line; (b) a plot S-parameters as a function of frequency.

The simulated S11 for the proposed glucose sensor, including the SIW together with a test solution sitting on the membrane-supported CSRR, is shown in Fig. 5a. Consistent with our calculated value, Fig. 5a suggests that the simulated resonant frequency is also 15.4 GHz when the sensing area of the proposed glucose sensor is fully filled with a test solution.

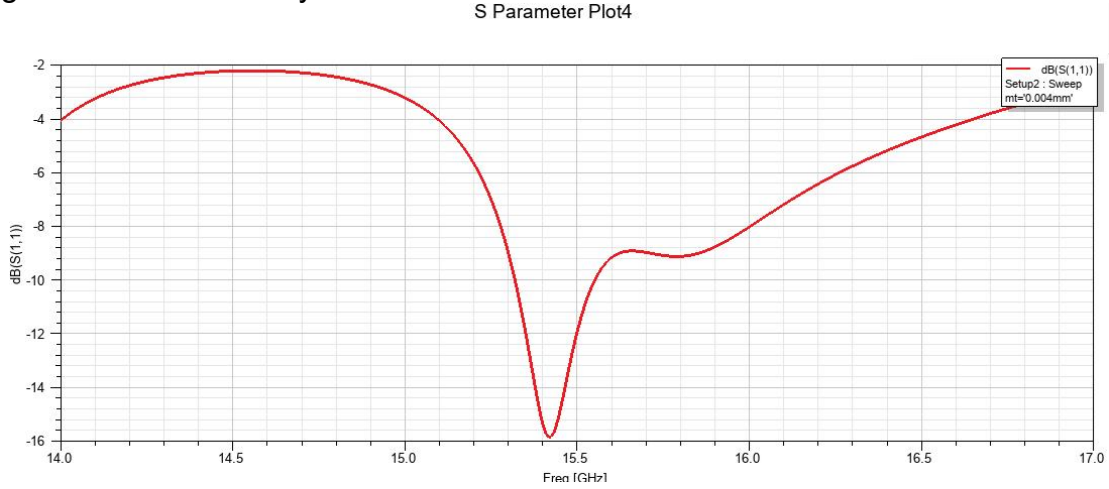

(a)

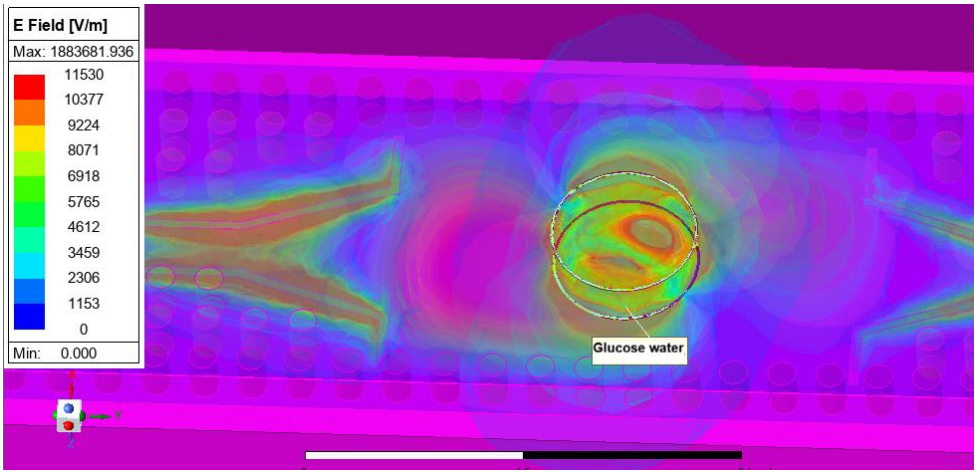

(b)

Fig. 5. Simulation results: (a) Simulated performance of the glucose sensor when the sensing area is loaded with a tap water. (b) 3-dimensional view of the simulated electric field distribution right at the interface between the CSRR and the FR4 membrane.

Fig. 5b shows the 3-dimensional view of the simulated electric field distribution right at the interface between the CSRR and the FR4 membrane. Because the thickness of the FR4 membrane is much less than the three-dimensional guided wavelength, which should be around 0.9mm, the electric field in the vertical direction is largely evanescent in nature. Most of the electromagnetic power is trapped in the FR4 membrane in the form of a spoof surface plasmon polariton along the interface between the glucose-water and the FR4 membrane. Once the recess in the sensing region is fully filled with the test solution, the discrepancy in the volume of the test solution filling the sensing region is expected to have non-zero but relatively less influential effects on the resonant frequency.

C) Sensitivity Analysis

The circular recess was filled with a glucose-water solution, of which the permittivity is much larger than that of FR4. In line with most of the dielectric waveguides, the electromagnetic energy should be preferentially stored in the recess or the sensing area. The liquid in the sensing region can be thought as a collection of different types of atoms, each of which is associated with its own resonance frequency (ω_j), damping factor (γ_j) and the oscillator strength (S_j). Here, j is just the index of the resonance corresponding to a particular type of atoms. The relative permittivity of the liquid can be readily modeled using Sellmeier Equation [8] as:

$$\varepsilon_r = 1 + \omega_{pm}^2 \sum_{j=0}^{M} \frac{S_j / S_0}{\omega_j^2 - \omega^2 - j\omega\gamma_j} \tag{3.1}$$

where ω_{pm} is the plasma frequency. Since the liquid in the sensing region is directly attached to the FR4 membrane and indirectly attached to the

complementary split-ring resonator, the plasma frequency should be the plasma frequency derived using equation (2.7). Accordingly, ω_{pm} becomes:

$$\omega_{pm} = 2\pi f_o = \frac{1}{\sqrt{L_t(C_g+C_{sur})}} \tag{3.2}$$

As emphasized previously, the surface plasma frequency f_o has already been determined to be around 15.1 GHz. At the surface plasma frequency, the electric field in the normal direction should be minimum, and the majority of the electromagnetic power is expected to be highly confined along the interface along the FR4 and the complementary split-ring resonator.

The surface plasma frequency (ω_{pm}or f_o) gives rise to a condition known as anomalous dispersion, under which the group velocity becomes greater than the speed of light, or even negative. As a result of this anomalous dispersive condition, there will be a perturbation in refractivity.

Suppose the operating frequency approaches a particular resonant frequency, ω_j. We can assume that $\omega=\omega_j$. Equation (3.1) can be reduced to:

$$\varepsilon_r=1+\omega_{pm}^2\left(j\frac{S_j/S_0}{\omega_j\gamma_j}\right) \tag{3.3}$$

Differentiating Equation (3.3) with respect to ω_j, we get:

$$\frac{d\varepsilon_r}{d\omega_j}=\left(\frac{\omega_{pm}}{\omega_j}\right)^2\left(-j\frac{S_j/S_0}{\gamma_j}\right) \tag{3.4}$$

Using the well-known chain rule in calculus, equation (3.4) can be rewritten as:

$$\frac{d\varepsilon_r}{d\omega_j}=\frac{d(\varepsilon'+j\varepsilon'')}{dC}\frac{dC}{d\omega_j}=\left(\frac{\omega_{p,m}}{\omega_j}\right)^2\left(-j\frac{S_j/S_0}{\gamma_j}\right) \tag{3.5}$$

where *C* is the concentration of the glucose solution in the recess under a anomalous dispersion. The sensitivity can be thought as a change of resonant frequency per unit concentration, i.e. $\frac{d\omega_j}{dC}$. The sensitivity should be a real number. It should not be imaginary. With a bit of algebraic re-arrangement, we can isolate the $d\omega_j/dC$ from equation (3.5) in the following manner:

$$\frac{d\omega_j}{dC}=\left(\frac{S_0}{S}\right)\gamma_j\left(\frac{\omega_j}{\omega_{pm}}\right)^2\frac{d}{dC}(\varepsilon'') \tag{3.6}$$

where γ_j, S, S_0, ω_{pm}, C respectively stand for the damping factor, the oscillator strength at resonant frequency (ω_j), the oscillator strength at the highest resonance, the plasma frequency and the glucose concentration.

Equation (3.6) suggests that the sensitivity of the glucose sensor is a function of the damping factor γ_j, the surface plasma frequency ω_{pm} , the resonant frequency ω_j.

The sensitivity is directly proportional to the damping factor (γ_j) caused by the conductivity of the glucose solution and the radiation resistance due to the antenna effects. Higher glucose concentration is in general indicative of a higher conductivity, which means a higher damping factor. The damping factor is inversely proportional to Q-factor. This Q-factor can be directly estimated by ratio of ($\frac{\omega_j}{\Delta\omega}$) over the frequencies in the neighborhood of the resonant frequency in the S11 plot.

In equation (3.6), one of most obvious factor influencing the sensitivity was obviously the ratio $\left(\omega_j/\omega_{pm}\right)$. For achieving a higher sensitivity, the plasma frequency, ω_{pm} ,should be minimized, whilst the resonant frequency, ω_j, should be maximized.

The term $\left(\omega_j/\omega_{pm}\right)$ in equation (3.6) also suggests that not all the resonances are equal. The resonant frequency is always lower than or equal to the plasma frequency. Assuming that there exists more than one resonant frequency in the system, equation (3.6) suggests that the resonances at lower frequencies tend to yield a lower sensing sensitivity.

D) Measurement Setup and Procedure

The performance of the proposed sensing device has been verified using the measurement setup as illustrated in Figs. 6a and 6b, where port 1 of the proposed sensor was connected to port 1 of a Rohde Schwarz vector network analyzer (ZVA 40), and port 2 of the same was terminated with a shunt resistor at 50 ohm.

Before conducting any measurement, a range of sample solutions of known glucose concentrations were prepared. During the measurement process, the sensing area (or the recess) of the proposed sensor was loaded with each of the samples using a pipette until the recess was fully filled (See Fig. 6b). The resulting S-parameters as displayed by ZVA 40 was then saved, whilst the resonant frequency was noted and recorded.

The concentrations of these samples include 0, 60mg/dL, 80mg/dL, 106mg/dL, 111mg/dL and 127mg/dL. The measurements have been replicated about 5 times but they were not done in one-go.

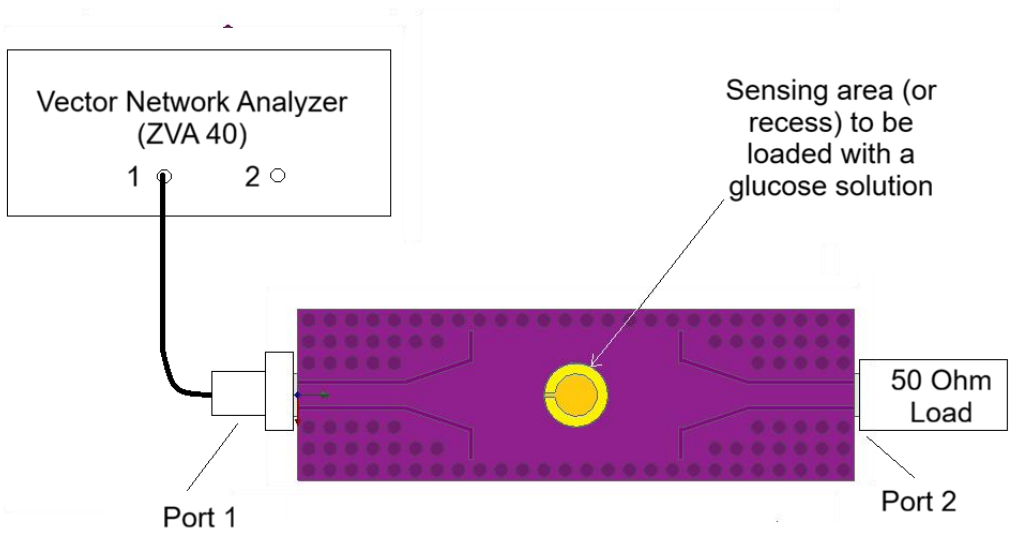

(a)

(b)

Fig 6. Measurement setup a) Schematic diagram; b) Photo of Our Experiment

Measured Results and Discussion

The main finding of this work is depicted in Fig. 7. The measured reflection coefficient (i.e. S11 parameter) for each of the sample glucose water has been plotted against frequency in Fig. 7a, whilst Fig. 7b shows a plot of resonant frequency as a function of glucose concentration. The resonant frequencies along the Y-axis of Fig. 7b were originally extracted from Fig. 7a.

At the first glance, the minima of the S11 in Fig. 7a look highly erratic, with virtually no observable linearity in the correlation between the magnitude of S11 and the glucose concentration. The irregular magnitudes of S11 among different samples have been observed because the measurements were done

at different times. On the other hand, the roles CSRR resonator are both a radiator and an absorbent of electromagnetic radiations. The ambient electromagnetic interference has changed from time to time. Under such a condition, the magnitudes of the minima of S11 were irregular and expected to be unstable.

After a closer look on the Fig. 7b, however, it was found that the correlation between the resonant frequency and the glucose concentration was almost 100% linear, with a Pearson correlation coefficient (r) reaching 0.99. The high linearity as observed in Fig. 7b suggests that the permittivity of the sensing region was relatively unaffected by the ambient electromagnetic interference.

The sensitivity was found to be 1.6 MHz/(mg/dL). Compared to counterparts as mentioned in Table 1, the sensitivity of the proposed was relatively high. The high sensitivity obtained in this work was attributed to the use of complementary split-ring resonator, which directly contributed a negative permittivity at a resonance.

Linearity is one of the most desired characteristics in sensing. With a highly linear sensing characteristic, a sensor usually exhibits a high measurement accuracy, high system stability and high post-measurement data processing efficiency. In this work, a high linearity was achieved even though the magnitudes of the reflective coefficient (S11) was erratic, unstable and subjected to the influences of unpredictable ambient electromagnetic interference.

The linearity of the proposed glucose sensor has been tested from 0 to a maximum glucose concentration of 127 mg/dL. Higher glucose concentrations have not been tested in this work. More research is needed to confirm if the linearity can be extended beyond 127 mg/dL.

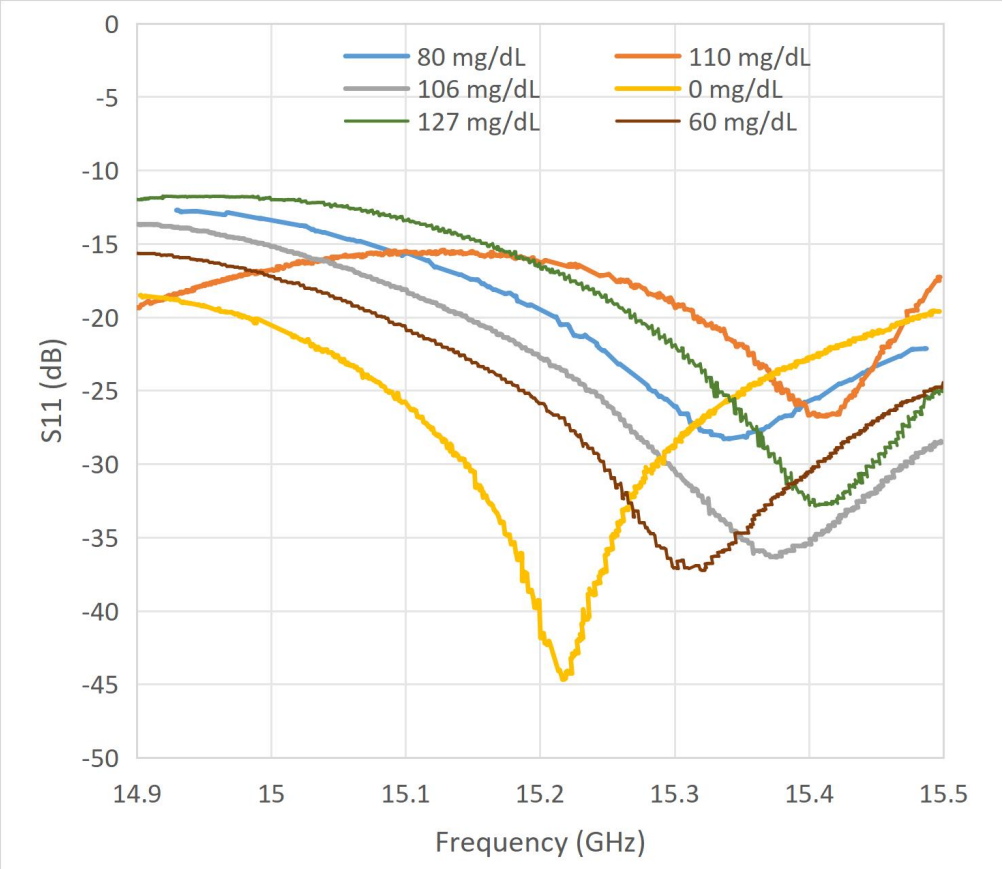
0
-5
-10
-15
-20
-25
-30
-35
-40
-45
-50
S11 (dB)
14.9
15
15.1
15.2
15.3
15.4
15.5
Frequency (GHz)
80 mg/dL
110 mg/dL
106 mg/dL
0 mg/dL
127 mg/dL
60 mg/dL

(a)

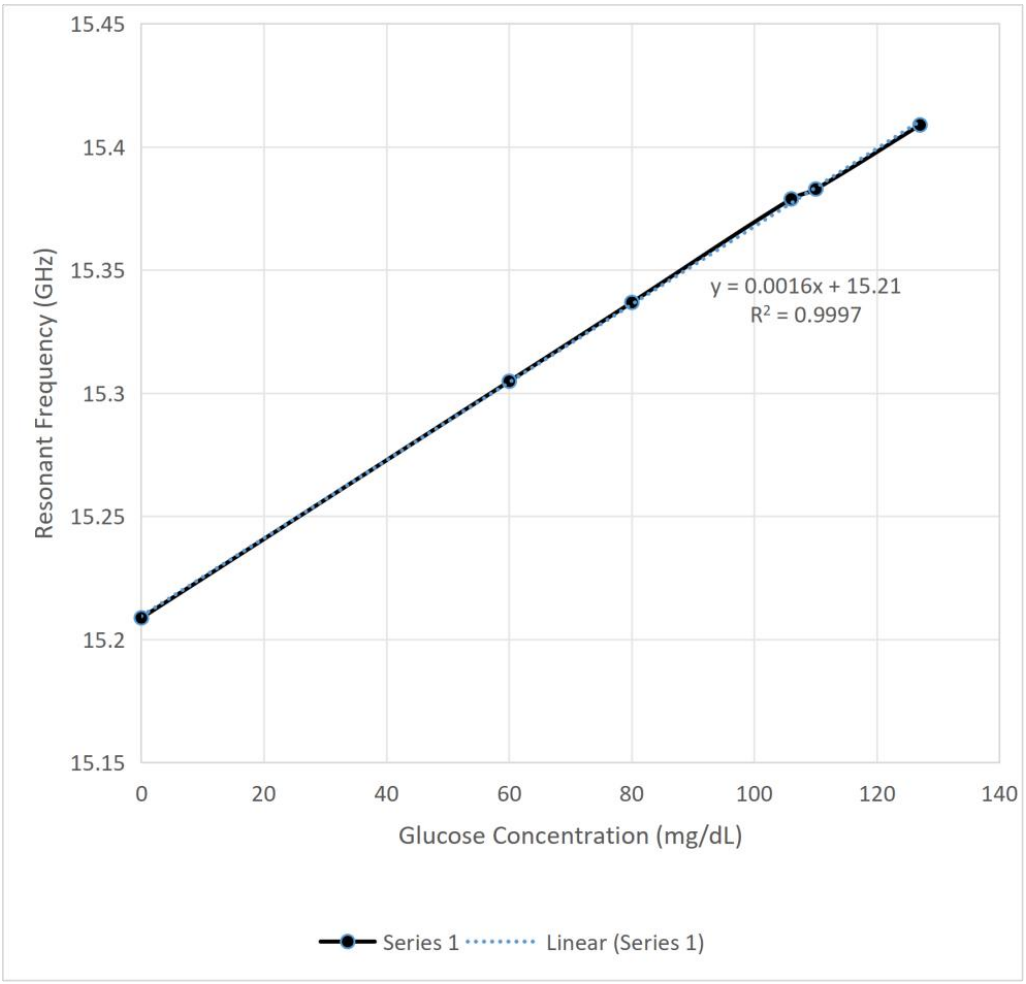

(b)

Fig. 7 Measured results: (a) S11 as a function of frequency for different glucose concentrations; (b) A plot of resonant frequency as a function of glucose concentration.

Conclusion

In this work, a substrate-integrated-waveguide (SIW) has been used in conjunction with a specially tailored membrane-supported resonator to form an ultra-linear glucose sensor. The proposed glucose sensor has exhibited an ultra-high linearity in the correlation between resonant frequency and glucose concentration, with a Pearson correlation coefficient (r) reaching 0.99, even though the S11 minima have unstable magnitudes. The sensitivity was found to be 1.6 MHz/(mg/dL).

Acknowledgement

This research is funded by the Vietnamese-German University under grant number DTCS2025-008.

References

1. Hamid Allah A, Ayissi Eyebe G, Domingue F. Improved Fully 3D-Printed SIW-Based Sensor for Non-Invasive Glucose Measurement. Sensors (Basel). 2025 Apr 9;25(8):2382. doi: 10.3390/s25082382. PMID: 40285071; PMCID: PMC12030663.
2. Ghosh, Prabir & Nayak, Avinash & Gorai, Abhik. (2025). Slit Capacitor-Based SIW Sensor with Dual Sensitivity for Non-Invasive Glucose Detection. 1-5. 10.1109/AESPC67542.2025.11326840.
3. Julián D. Ortiz, Juan D. Baena, Ricardo Marqués, Amarachukwu N. Enemuo, Jonah Gollub, Roman, Akhmechet, Boyan Penkov, Chris Sarantos, and David T. Crouse, Babinet's principle and saturation of the resonance frequency of scaled-down complementary metasurfaces, Appl. Phys. Lett. 118, 221901 (2021); https://doi.org/10.1063/5.0048960
4. S. Moitra, S. Nayak, R. Regar, S. Kumari, K. Kumari, F. Parween and F. Naseem, “Circular Complementary Split Ring Resonators (CSRR) based SIW BPF”, 2019 Second International Conference on Advanced Computational and Communication Paradigms (ICACCP), 2019
5. Sydoruk, Oleksiy & Tatartschuk, E. & Shamonina, E. & Solymar, Laszlo. (2009). Analytical formulation for the resonant frequency of split rings. Journal of Applied Physics. 105. 014903 - 014903. 10.1063/1.3056052.
6. Cadence Design System, “Single Split-Ring Resonator Design”, Retrieved on 29 April, 2026, Retrieve from https://resources.system-analysis.cadence.com/blog/msa2021-single-split-ring-resonator-design
7. Smolyaninov, I., Balzano, Q. & Kozyrev, A. B. Surface electromagnetic waves at seawater-air and seawater-seafloor interfaces. IEEE Open. J. Antennas Propag. 4, 51–59 (2023).
8. Baird, C. Lecture 2 Notes, Electromagnetic Theory II (University of Massachusetts, 2024).
9. H. M. Marzouk, A. S. A. El-Hameed, A. Allam, R. K. Pokharel and A. B. Abdel-Rahman, "Substrate Integrated Waveguide Sensor for Noninvasive Glucose Measurement," 2023 11th International Japan-Africa Conference on Electronics, Communications, and Computations (JAC-ECC), Alexandria, Egypt, 2023, pp. 46-49, doi: 10.1109/JAC-ECC61002.2023.10479616.
10. Ameer B. Alsultani, Hussam Al-Saedi, Omer S. Alkhafaf, Katalin Kovács, J. Geoffrey Chase, Balazs Benyo, Development and experimental evaluation of single-port substrate integrated waveguide resonator with dual-parameter sensitivity for non-invasive blood glucose monitoring, Measurement, Volume 278, 2026, 121635, ISSN 0263-2241, https://doi.org/10.1016/j.measurement.2026.121635.
11. Mohd Bahar, A.A., Zakaria, Z., Md. Arshad, M.K. et al. Real Time Microwave Biochemical Sensor Based on Circular SIW Approach for Aqueous Dielectric Detection. Sci Rep 9, 5467 (2019). https://doi.org/10.1038/s41598-019-41702-3